

Static quark anti-quark pair in $SU(2)$ gauge theory

Alexei Bazavov

Department of Physics, University of Arizona, Tucson, AZ 85721, USA

Péter Petreczky

*RIKEN-BNL Research Center and Physics Department,
Brookhaven National Laboratory, Upton NY 11973, USA*

Alexander Velytsky

*Enrico Fermi Institute, University of Chicago, 5640 S. Ellis Ave., Chicago, IL 60637, USA, and
HEP Division and Physics Division, Argonne National Laboratory, 9700 Cass Ave., Argonne, IL 60439, USA*

We study singlet and triplet correlation functions of static quark anti-quark pair defined through gauge invariant time-like Wilson loops and Polyakov loop correlators in finite temperature $SU(2)$ gauge theory. We use the Lüscher-Weisz multilevel algorithm, which allows to calculate these correlators at very low temperatures. We observe that the naive separation of singlet and triplet states in general does not hold non-perturbatively, however, is recovered in the limit of small separation and the temperature dependence of the corresponding correlators is indeed very different.

I. INTRODUCTION

It is well established that strongly interacting matter undergoes a deconfining transition at some temperature which is triggered by large increase in number of degrees of freedom (e.g. large increase in the entropy density) as well as melting of hadronic degrees of freedom. One of the most important feature of the deconfined phase is the screening of color charges. It has been argued that color screening will lead to quarkonium dissociation above the deconfinement temperature which can be used as a signature of quark gluon plasma formation in heavy ion collisions [1]. Melting of quarkonium states can be rigorously studied in terms of spectral functions. Attempts to reconstruct spectral functions from Euclidean time quarkonium correlators calculated on the lattice have been presented in Refs. [2, 3, 4] (for light mesons see [5, 6, 7]). These studies seemed to indicate that charmonium states may survive up to unexpectedly high temperatures $1.6T_c - 2.2T_c$ (T_c being the transition temperature). However, it turns out that reconstruction of the spectral function is difficult [8]. The only statement that can be made with confidence is that the Euclidean time quarkonium correlation functions do not show significant temperature dependence [8].

On the lattice color screening is usually studied in terms of the Polyakov loop correlator related to the free energy of static quark anti-quark pair [9]. Unlike quarkonium correlators it shows very significant temperature dependence across the deconfinement transition. In fact, in the deconfined phase the free energy of static quark anti-quark pair shows large temperature dependence even for very small separations between the static quark and anti-quark, much smaller than the inverse temperature [10, 11, 12]. In perturbative picture this can be understood due to the fact that in the deconfined phase not only singlet quark anti-quark ($Q\bar{Q}$) states contribute to the free energy but also colored states with $Q\bar{Q}$ in the

adjoint (octet for $SU(3)$ and triplet for $SU(2)$) representation. This observation is also supported by lattice calculations of the correlation function of two temporal Wilson lines in Coulomb gauge, which in perturbation theory corresponds to the so-called singlet free energy [13, 14, 15, 16, 17, 18, 19]. The singlet free energy is temperature independent at short distances and coincides with the zero temperature potential as expected. However, at larger distances, e.g. distances of the order of typical quarkonium size, it also shows significant temperature dependence. Thus there seems to be a puzzle: heavy quarkonium correlators show almost no temperature dependence, while static mesons are largely affected by the deconfined medium.

In the past several years quarkonium properties at finite temperature have been studied in potential models which use the singlet free energy as an input [20, 21, 22, 23, 24, 25, 26]. Furthermore, within potential model calculations it has been shown that the small temperature dependence of the quarkonium spectral function does not necessarily imply survival of quarkonium states at high temperatures [25, 26]. Most quarkonium states are melted due to color screening as it was originally suggested by Matsui and Satz but threshold enhancement can compensate for absence of bound states [25, 26].

Potential models can be justified in the effective field theory framework, the potential non-relativistic QCD (pNRQCD), where both scales related to the heavy quark mass and bound state size are integrated out [27]. This approach can be generalized to finite temperature, where also the thermal scales (the temperature and the Debye mass) have to be eventually integrated out [28]. In pNRQCD both color singlet and color octet $Q\bar{Q}$ states are present as an effective degrees of freedom. The problem of defining color singlet and adjoint $Q\bar{Q}$ states on the lattice has been considered in Ref. [29]. It has been found that the conventional definition of singlet and adjoint states have problems. Since this question is very

relevant for quarkonium physics at finite temperature as well as from purely conceptual point of view a more detailed study is needed.

In this paper we study static meson correlators in 4 dimensional $SU(2)$ gauge theory at finite temperature and show how the problem observed in Ref. [29] can be resolved in the limit of small distances and/or high temperatures. The rest of the paper is organized as follows. In section II we discuss static meson correlators at finite temperature and their interpretation in the limit of high and low temperatures. Section III contains our numerical results along with some important technical details. Finally in section IV we give our conclusions.

II. STATIC MESON CORRELATORS

Following Ref. [29] we start our discussion considering static meson operators in color singlet and adjoint (triplet) states

$$O(x, y; t) = \bar{\psi}(x, t)U(x, y; t)\psi(y, t) \quad (1)$$

$$O^\alpha(x, y; t) = \bar{\psi}(x, t)U(x, x_0; t)T^\alpha U(x_0, y; t)\psi(y, t), \quad (2)$$

where T^α is the group generator, $\bar{\psi}$ and ψ are creation and annihilation operators of static quarks and $U(x, y; t)$ are the spatial gauge transporters. In this section we consider the general case of $SU(N)$ group, although the numerical calculations have been done for $N = 2$. Next we consider correlators of these static meson operators at time $t = 1/T$ which after integrating out the static fields have the form [29]:

$$G_1(r, T) = \frac{1}{N} \langle \text{Tr} L^\dagger(x) U(x, y; 0) L(y) U^\dagger(x, y, 1/T) \rangle, \quad (3)$$

$$G_a(r, T) = \frac{1}{N^2 - 1} \langle \text{Tr} L^\dagger(x) \text{Tr} L(y) \rangle - \frac{1}{N(N^2 - 1)} \langle \text{Tr} L^\dagger(x) U(x, y; 0) L(y) U^\dagger(x, y, 1/T) \rangle, \quad (4)$$

$r = |x - y|.$

Here $L(x)$ is the temporal Wilson line, which on the lattice is simply $L(x) = \prod_{\tau=0}^{N_\tau-1} U_0(x, \tau)$ with $U_0(x, \tau)$ being the temporal links. The correlators depend on the choice of the spatial transporters $U(x, y; t)$. Typically a straight line connecting points x and y is used as a path in the gauge transporters, i.e. one deals with time-like rectangular cyclic Wilson loops, i.e. Wilson loops wrapping around the time direction. This object has been calculated at finite temperature in hard thermal loop (HTL) perturbation theory in context of re-summed perturbative calculations of quarkonium spectral functions [30, 31, 32]. This is one of the reasons we are interested in non-perturbative evaluation of it. In the special gauge, where $U(x, y; t) = 1$ the above correlators give standard definition of the so-called singlet and adjoint free energies

$$\exp(-F_1(r, T)/T) = \frac{1}{N} \langle \text{Tr} L^\dagger(x) L(y) \rangle, \quad (5)$$

$$\exp(-F_a(r, T)/T) = \frac{1}{N^2 - 1} \langle \text{Tr} L^\dagger(x) \text{Tr} L(y) \rangle - \frac{1}{N(N^2 - 1)} \langle \text{Tr} L^\dagger(x) L(y) \rangle. \quad (6)$$

The singlet and triplet free energies can be calculated at high temperature in leading order HTL approximation [33] resulting in:

$$F_1(r, T) = -\frac{N^2 - 1}{2N} \frac{\alpha_s}{r} \exp(-m_D r) - \frac{(N^2 - 1)\alpha_s m_D}{2N}, \quad (7)$$

$$F_a(r, T) = +\frac{1}{2N} \frac{\alpha_s}{r} \exp(-m_D r) - \frac{(N^2 - 1)\alpha_s m_D}{2N}, \quad (8)$$

with $m_D = gT\sqrt{(N/3)}$ being the leading order Debye mass. At this order F_1 and F_a are gauge independent or in other words do not depend on the choice of the parallel transporters $U(x, y; t)$. Note that at small distances ($rm_D \ll 1$) the singlet free energy

$$F_1(r, T) \simeq -\frac{N^2 - 1}{2N} \frac{\alpha_s}{r} \quad (9)$$

is temperature independent and coincides with the zero temperature potential, while the adjoint free energy

$$F_a(r, T) \simeq \frac{1}{2N} \frac{\alpha_s}{r} - \frac{N}{2} \alpha_s m_D \quad (10)$$

depends on the temperature.

The physical free energy of a static quark anti-quark pair, i.e. the one related to the work that has to be done to separate the static charges by certain distance is given by the thermal average of the singlet and adjoint free energies [9]

$$\begin{aligned} \exp(-F(r, T)/T) &= \\ &= \frac{1}{N^2} \exp(-F_1(r, T)/T) + \frac{N^2 - 1}{N^2} \exp(-F_a(r, T)/T) \\ &= \frac{1}{N^2} \langle \text{Tr} L(x) \text{Tr} L(y) \rangle \equiv \frac{1}{N^2} G(r, T). \end{aligned} \quad (11)$$

This quantity is explicitly gauge independent. In leading order HTL approximation the free energy is

$$F(r, T) = -\frac{(N^2 - 1)}{4N^2} \frac{\alpha_s^2}{r^2 T} \exp(-2m_D r). \quad (12)$$

The $1/r^2$ behavior is due to partial cancellation between the singlet and adjoint contribution [9, 34] and has been confirmed by lattice calculations in the intermediate distance regime above deconfinement [12, 15].

Using the transfer matrix one can show that in the confined phase [29]

$$G_1(r, T) = \sum_{n=1}^{\infty} c_n(r) e^{-E_n(r, T)/T}, \quad (13)$$

$$G(r, T) = \sum_{n=1}^{\infty} e^{-E_n(r, T)/T}, \quad (14)$$

where E_n are the energy levels of static quark and anti-quark pair. The coefficients $c_n(r)$ depend on the choice of U entering the static meson operator O in Eq. (1). Since the color averaged correlator $G(r, T)$ corresponds to a measurable quantity (at least in principle) it does not contain c_n . The lowest energy level is the usual static quark anti-quark potential, while the higher energy levels correspond to hybrid potentials [35, 36, 37, 38]. Using multi-pole expansion in pNRQCD one can show that at short distances the hybrid potential corresponds to the adjoint potential up to non-perturbative constants [27]. Indeed, lattice calculations of the hybrid potentials indicate a repulsive short distance part [35, 36, 37, 38]. If $c_1 = 1$ the dominant contribution to G_a would be the first excited state E_2 , i.e. the lowest hybrid potential which at short distances is related to the adjoint potential. In this sense G_a is related to static mesons with $Q\bar{Q}$ in adjoint state. Numerical calculations show, however, that $c_1(r) \neq 1$ and depends on the separation r . Thus G_a also receives contribution from E_1 [29]. The lattice data seem to suggest that c_1 approaches unity at short distances [29] in accord with expectations based on perturbation theory, where $c_1 = 1$ up to $\mathcal{O}(g^6)$ corrections [27]. Therefore at short distances, $r \ll 1/T$ the color singlet and color averaged free energy are related $F(r, T) = F_1(r, T) + T \ln(N^2 - 1)$. This relation is indeed confirmed by lattice calculations [14]. In the next section we are going to study the singlet and averaged correlators G_1 and G in the confined phase and extract the coefficients c_1 .

III. NUMERICAL RESULTS

We have calculated correlation functions of static mesons $G_1(r, T)$ and $G(r, T)$ both in the confined and deconfined phase of $SU(2)$ gauge theory. In our calculations we used the Lüscher-Weisz algorithm for noise reduction [39], which makes possible to calculate these correlators at low values of temperature T not accessible by standard methods. Calculations have been done for $\beta = 4/g^2 = 2.5$ and 2.7 using lattices with spatial extent $N_s = 24$ and $N_s = 32$. Gauge configurations have been generated using combination of heat-bath and over-relaxation algorithms. Measurements are taken after 2 complete updates. A complete update consists of one heat-bath and two over-relaxation updates of the entire lattice and hundred slice updates, in which all links inside a slice $N_s^3 \times 2$ except of the boundary are updated for all $N_\tau/2$ slices with heat-bath.

We have studied the color singlet and averaged correlators given by Eqs. (3) and (11). The spatial links entering the transporter $U(x, y; 0)$ were smeared using APE smearing [40], which has been applied iteratively. The weight of the staple in the APE smeared link was 0.12. For $\beta = 2.5$ we use spatial links with 10 steps of APE smearing and unsmeared spatial links. For $\beta = 2.7$ we used unsmeared spatial links as well as spatial links

with 10 steps and 20 steps of APE smearing. The lattice spacing has been set using the string tension calculated in Ref. [38] $a^2\sigma_{\beta=2.5} = 0.0363(3)$ and $a^2\sigma_{\beta=2.7} = 0.0112(2)$. When quoting the results in terms of reduced temperature T/T_c we use the value $T_c/\sqrt{\sigma} = 0.69(2)$ [41]. The simulation parameters, including the different levels of APE smearing used in the present study are summarized in Table I.

For comparison with the study of static meson correlation functions in Coulomb gauge [15] we have also performed calculations on $16^3 \times 4$ lattice at $\beta = 2.3533$ and 2.4215 . The two gauge coupling correspond to temperatures $1.2T_c$ and $1.5T_c$ respectively (see Ref. [15] for details). Here we used 5, 10 and 20 APE smearings. The results from these calculations will be discussed in section III C.

A. Color averaged correlator in the confined phase

The color averaged correlator has been calculated in the confined phase in the temperature interval $0.32T_c - 0.95T_c$ $\beta = 2.5$ and $0.49T_c - 0.98T_c$ for $\beta = 2.7$. Thus we study this correlator also at very low temperatures, where they have not been calculated before. The numerical results for the color averaged free energy for $\beta = 2.5$ are shown in Figure 1. To eliminate the trivial temperature dependence due to the color trace normalization in Figure 1 we show the subtracted free energy $F'(r, T) = F(r, T) - T \ln 4$, see the discussion in the previous section. In the figure also the zero temperature potential calculated in Ref. [38] is shown. The color averaged free energy does not show any temperature dependence up to temperatures of about $0.76T_c$. For $T = 0.76T_c$ the color averaged free energy is below the zero temperature potential, indicating a decrease in the effective string tension in accordance with earlier studies (see e.g. [10, 15]). We see even larger change closer to the transition temperature, namely for $T \geq 0.95T_c$.

Since the temperature dependence for $T < 0.76T_c$ is relatively small we attempted to fit the color averaged correlator with the 1-exponential form $G(r, T) = c_1^q(r) \exp(-E_1(r)/T)$. The ground state energy $E_1(r)$ extracted from this fit agrees well with the zero temperature potential calculated in Ref. [38], while the coefficients $c_1^q(r)$ are close to one as expected (see the discussion in the previous section). The fit details are shown in the Appendix. Although the deviations of $c_1^q(r)$ from unity are small, they appear to be statistically significant. These deviations increase with increasing r . Therefore they are likely to be due to the contribution from excited states, as the gap between the ground state and excited states (hybrid potential) gets smaller with increasing separation. Therefore we attempted to fit the color averaged correlator with 2-exponential form $G(r, T) = \exp(-E_1(r)/T) + \exp(-E_2(r)/T)$ using $T < 0.76T_c$. The results of the fit are given in the Appendix. We find that the value of E_1 extracted from the 2-exponential fits are

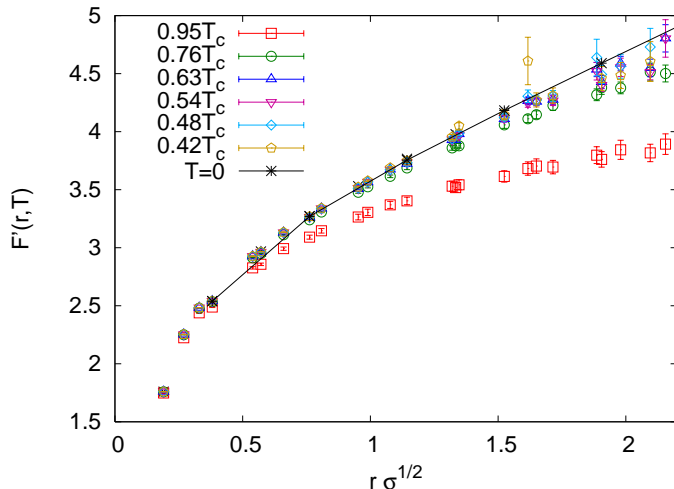


FIG. 1: The color averaged free energy defined by Eq. (11) below deconfinement temperature at $\beta = 2.5$ calculated on $32^3 \times N_\tau$ lattices. Also shown is the $T = 0$ potential.

consistent with the ones obtained from 1-exponential fit as well as with the value of the zero temperature potential. For $E_2(r)$ we find values which are somewhat below the first hybrid potential. This is presumably due to the fact that there is small contribution from the higher excited states.

B. Color singlet correlators in the confined phase

As mentioned above the color singlet correlators have been calculated using different levels of APE smearing in the spatial gauge connection. It is well known that smearing increases the overlap with the ground state by removing the short distance fluctuation in the spatial links (see e.g. [42]). For this reason smearing also reduces the breaking of the rotational invariance to the level expected in the free theory. We have found that when no smearing is used the color singlet free energy, $-T \ln G_1(r, T)$ shows a small but visible temperature dependence. In particular $F_1(r, T)$ is larger than the $T = 0$ potential for intermediate distances $0.5 < r\sqrt{\sigma} < 2$. A similar effect has been observed in calculation in 3 dimensional $SU(2)$ gauge theory [29, 43] as well in 4 dimensional $SU(2)$ and $SU(3)$ gauge theory calculations in Coulomb gauge [15, 44]. The temperature dependence of the singlet free energy is significantly reduced when APE smearing is applied. In Figure 2 we show the color singlet free energy for $\beta = 2.5$ and 10 APE smearings. As one can see from the figure the color singlet free energy shows significantly smaller temperature dependence as we get closer to the deconfinement temperature. In particular, only for $T = 0.95T_c$ we see significant temperature dependence, which, however, is much smaller than for color averaged free energy. To understand the temperature dependence of the color singlet correlator we use

$\beta = 2.5$					$\beta = 2.7$				
N_s	N_τ	T/T_c	N_{APE}	# meas	N_s	N_τ	T/T_c	N_{APE}	# meas
32	4	1.90	0	4K	32	4	3.42	0	4K
32	4	1.90	10	1K	32	4	3.42	10, 20	1K
32	6	1.27	0	4K	32	6	2.28	0	4K
24,32	6	1.27	10	1K,1K	32	6	2.28	10, 20	1K
24,32	8	0.95	0	16K,4K	32	8	1.71	0	4K
24,32	8	0.95	10	1K,1K	32	8	1.71	10, 20	1K
24,32	10	0.76	0	8K,4K	32	10	1.37	0	8K
24,32	10	0.76	10	1K,1K	32	10	1.37	10, 20	1K
24,32	12	0.63	0	8K,4K	32	12	1.14	0	8K
24,32	12	0.63	10	1K,1K	32	12	1.14	10, 20	1K
24,32	14	0.54	0	4K,4K	32	14	0.98	0	8K
24,32	14	0.54	10	1K,1K	32	14	0.98	10, 20	1K
24,32	16	0.48	0	4K,4K	32	16	0.86	0	4K
24,32	16	0.48	10	1K,1K	32	16	0.86	10, 20	1K
24,32	18	0.42	0	8K,4K	32	18	0.76	0	8K
24,32	18	0.42	10	1K,1K	32	18	0.76	10, 20	1K
24,32	20	0.38	0	8K,4K	32	20	0.68	0	4K
24,32	20	0.38	10	1K,1K	32	20	0.68	10, 20	1K
24,32	22	0.35	0	8K,4K	32	22	0.62	0	4K
24,32	22	0.35	10	1K,1K	32	22	0.62	10, 20	1K
32	24	0.32	0	4K	32	24	0.57	0	4K
32	24	0.32	10	1K	32	24	0.57	10, 20	1K
					32	28	0.49	0	4K
					32	28	0.49	10, 20	1K

TABLE I: Simulation parameters, # meas refers to the actual number of measurements.

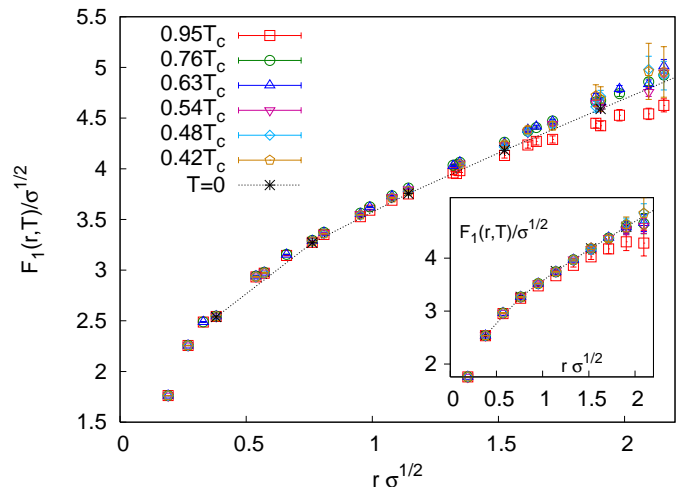


FIG. 2: The color singlet free energy below deconfinement temperature at $\beta = 2.5$ calculated on $32^3 \times N_\tau$ lattices. Also shown is the $T = 0$ potential. The inset shows the color singlet free energy from which the contribution from the matrix element $T \ln c_1$ has been subtracted.

1-exponential fit $G_1(r, T) = c_1(r) \exp(-E_1(r)/T)$. In all cases considered, the value of $E_1(r)$ extracted from fits are in good agreement with the calculation of the zero temperature potential in Ref.[38]. The value of the prefactor $c_1(r)$ is shown in Figure 3. When no APE smearing is used the value of $c_1(r)$ strongly depends on the separation r . At small distances it shows a tendency of approaching unity as one would expect in perturbation theory. However, $c_1(r)$ decreases with increasing distance r . At large distance its value is around 0.3 – 0.5 (see Appendix for details). Similar results for $c_1(r)$ have been obtained in study of $SU(2)$ gauge theory in 3 dimensions [29]. When APE smearing is applied the r -dependence of the amplitude $c_1(r)$ is largely reduced and its value is close to unity both for $\beta = 2.5$ and $\beta = 2.7$. For $\beta = 2.7$ we also see that increasing the number of smearing steps from 10 to 20 reduces the deviation of $c_1(r)$ from unity.

As discussed in section II perturbation theory predicts that the deviations of $c_1(r)$ from unity is of order α_s^3 . Therefore it can be made arbitrarily small by going to sufficiently small distances but even for distances accessible in this study these deviations are expected to be small based on perturbation theory. It is known, however, that lattice perturbation theory converges very poorly. The main reason for this has been identified with the short distance fluctuations of link variables, which makes their mean value very different from unity [45]. Smearing removes these short distance fluctuations and this is the reason why $c_1(r)$ is much closer to unity when APE smearing is applied.

From the above discussions it is clear that almost the entire temperature dependence of the singlet free energy at distances $0.5 < r\sqrt{\sigma} < 2$ is due to the deviation of c_1 from unity and can be largely reduced by applying APE smearing to the links in the spatial gauge connections. To further demonstrate this point in the inset of Figure 2 we show the results for $F_1(r, T) + T \ln c_1(r)$. Clearly no temperature dependence can be seen in this quantity up to $0.95T_c$, where we see temperature dependence at distances $r\sqrt{\sigma} \geq 1.5$ corresponding the expected drop of the effective string tension.

C. Color singlet free energy in the deconfined phase

In this subsection we discuss the properties of the color singlet free energy, $F_1(r, T) = -T \ln G_1(r, T)$ above the deconfinement temperature. It turns out that the singlet free energy calculated from cyclic Wilson loops shares the same qualitative features as the singlet free energy calculated in Coulomb gauge [14, 15, 16, 17, 18]. At short distances it is temperature independent and coincides with the zero temperature potential. At large distances it approaches a constant $F_\infty(T)$ which monotonically decreases with the temperature. The constant $F_\infty(T)$ is the free energy of two isolated static quarks, or equivalently of a quark anti-quark pair at infinite separation.

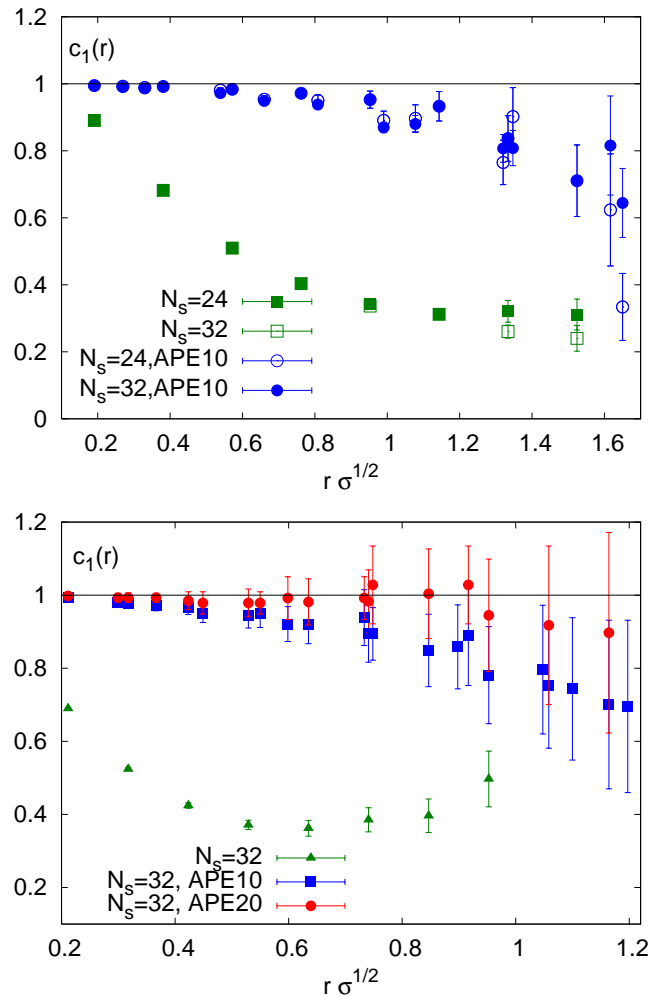


FIG. 3: The pre-exponential factor of the color singlet correlators as function of distance r for $\beta = 2.5$ (top) and $\beta = 2.7$ (bottom). Shown are results for unsmearred spatial links and 10 and 20 steps of APE smearing.

Its value is therefore independent of the definition of the singlet correlator $G_1(r, T)$ and is related to the renormalized Polyakov loop $L_{ren}(T) = \exp(-F_\infty(T)/(2T))$ [14].

At leading order $F_1(r, T) - F_\infty(T)$ is of Yukawa form (c.f. Eq. (7)). Therefore we find it useful to show our numerical results in terms of the screening function

$$S(r, T) = r \cdot (F_1(r, T) - F_\infty(T)) \quad (15)$$

In Figure 4 we show the results for the screening function at different temperatures. At short distances ($rT < 0.5$) the singlet free energy does not depend on the smearing level. Furthermore, it is very close to the free energy calculated in Coulomb gauge. We expect that at large distances the screening function $S(r, T)$ will show an exponential decay determined by a temperature dependent screening mass $m_1(T)$, which is equal to the leading order Debye mass up to the non-perturbative g^2 corrections: $m_1 = m_D + \mathcal{O}(g^2)$ [46]. From Fig. 4 we can see

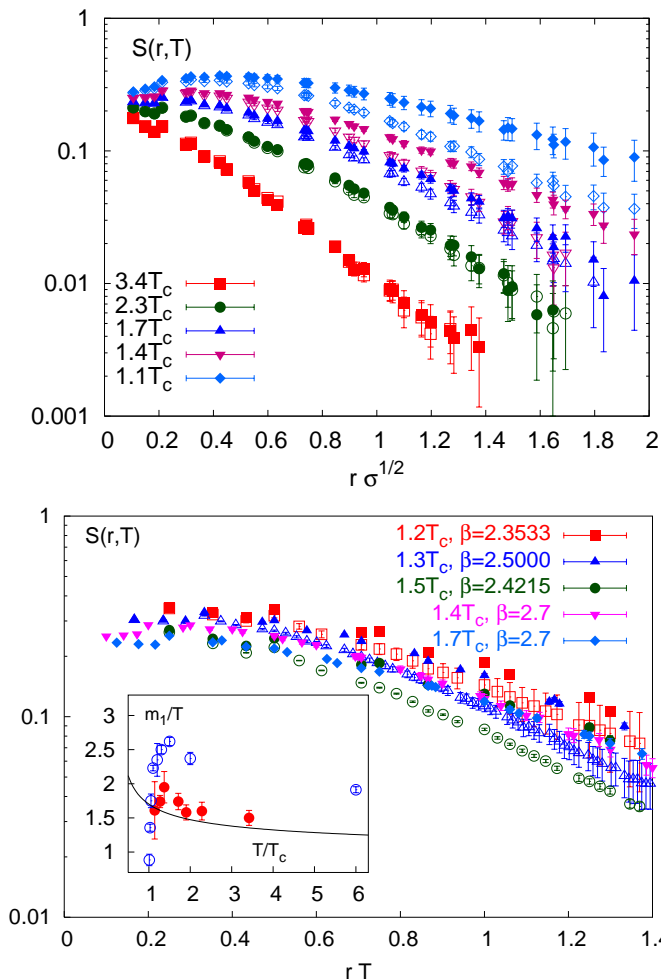


FIG. 4: The screening function $S(r, T) = r(F_1(r, T) - F_\infty(T))$ at different temperatures calculated for $\beta = 2.7$ as function of the distance in units of $\sqrt{\sigma}$ (top) and as function of rT and different values of β (bottom). In the lower panel we also shown the results from calculations in Coulomb gauge [15] as open symbols. In the inset the screening masses m_1 extracted from singlet free energies are shown together with the results obtained in Coulomb gauge [15] (open symbols). The line shows the leading order results for the Debye mass. In the upper panel the filled symbols correspond to 20 APE smearings steps, while the open ones to 10 APE smearings steps.

that indeed $S(r, T)$ behaves exponentially with screening mass proportional to the temperature. We note, however, that there is some dependence on the smearing level at larger distances. This disappears at high temperatures and with increasing the smearing level. In particular, for $\beta \leq 2.5$ it turns out that there is no dependence on smearing level for 5 or more smearing steps. For $\beta = 2.7$ we need 10-20 steps depending on the temperature to achieve stable results. Fitting the large distance behavior of the screening function by an exponential form $\exp(-m_1(T)r)$ we determine the screening mass $m_1(T)$. Typically we considered distances $r > 1/T$ as well as the

maximal number of smearings steps (10 for $\beta \leq 2.5$ and 20 for $\beta = 2.7$) in our fits. In the inset of Fig. 4 we show the color singlet screening masses extracted from the fits and compare them to the results obtained in Coulomb gauge in Ref. [15]. In the inset we also show the leading order Debye mass calculated using 2-loop gauge coupling $g(\mu = 2\pi T)$ in \overline{MS} -scheme. We used the value $T_c/\Lambda_{\overline{MS}} = 1.09$ [47] to calculate the coupling g . As we see from the figure the screening masses are smaller than those calculated in Coulomb gauge and agree well with the leading order perturbative prediction.

Leading order perturbation theory also predicts that $F_1^2(r, T)/F(r, T) = 6$ for $r > 1/T$ (c.f. Eqs. 7-8). We find that at the highest temperature, $T = 3.42T_c$ this relation indeed holds within statistical errors.

D. Color triplet free energy

We have calculated the color triplet correlator defined by Eq. (4) for different temperatures below and above the transition temperature. Below the deconfinement temperature we observe a moderate T -dependence of the triplet correlator. We also find that the corresponding free energy $-T \ln G_3(r, T)$ is smaller than the first hybrid potential calculated in Ref. [38], but larger than the triplet free energy in Coulomb gauge [15].

Let us assume that only two states contribute to the Eqs. (13) and (14). Then from Eq. (4) it follows that

$$F_3(r, T) = E_2(r) - T \ln(1 - c_2(r) + \frac{1}{3}(1 - c_1(r))e^{\Delta E(r)/T}), \quad (16)$$

with $\Delta E(r) = E_2(r) - E_1(r)$. We have seen in section III.B that the temperature dependence of the singlet free energy is quite small. In any case it is considerably smaller than the temperature dependence of the averaged free energy. Therefore the contribution of the excited states to $G_1(r, T)$ is quite small and it is reasonable to assume that $c_2(r) \ll 1$. We also expect that at small distances, $c_2(r) \sim (r\Lambda_{QCD})^4$ [48]. Thus, the temperature dependence of $F_3(r, T)$ and its deviation from the hybrid state $E_2(r)$ is due to small deviation of $c_1(r)$ from unity. At low temperatures, when $\Delta E \gg T$ these small deviations are amplified by the exponential factor. To verify this, we have subtracted the correction $T \ln(1 + \frac{1}{3}(1 - c_1)e^{\Delta E/T})$ from the triplet free energy assuming that $E_1(r)$ is given by the ground state potential and $E_2(r)$ is given by the first hybrid potential as calculated in Ref. [38]. The numerical results are summarized in Fig. 5 which shows that after this correction is accounted for in the confined phase the triplet free energy at low temperatures agrees reasonably well with the first hybrid potential. As temperature increases more excited states contribute. In particular, at $0.76T_c$ the value of the triplet free energy can be accounted for by including the next hybrid state [38]. However, at $0.95T_c$ we see large temperature effects, which cannot be explained by including the contribution from only few excited states.

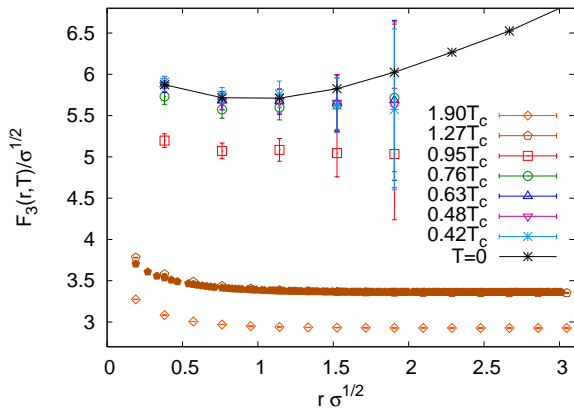


FIG. 5: The triplet free energy at different temperatures calculated at $\beta = 2.5$. The filled symbols correspond to calculations in Coulomb gauge. Also shown is the first hybrid potential calculated in Ref. [38].

In Fig. 5 we also show the triplet free energy above the deconfinement temperature compared to the calculations in Coulomb gauge [15]. It turns out to be much smaller than in the confined phase and agrees well with Coulomb gauge results. This means that the small deviation of the overlap factor $c_1(r)$ from unity are unimportant in this case. The triplet free energy monotonically decreases with increasing temperature as expected in HTL perturbation theory (c.f. Eq. (8)). In the limit of high temperatures and short distances $r < 1/T$ we have $E_2(r) = \alpha_s/(4r)$, $\Delta E(r) = \alpha_s/r$, $c_2(r) \simeq 0$ and $c_1(r) = 1 + \mathcal{O}(\alpha_s^3)$. Therefore we can expand the logarithm in Eq. (16) to get

$$F_3(r, T) = +\frac{1}{4} \frac{\alpha_s}{r} + \mathcal{O}(\alpha_s^3 T) + \mathcal{O}(\alpha_s m_D). \quad (17)$$

Thus the correction due to $c_1(r) \neq 0$ are much smaller than the expected leading order thermal effects in the triplet free energy.

While the temperature dependence of $F_3(r, T)$ and $F_1(r, T)$ is different even at short distances the r -dependence is expected to be similar. In leading order perturbation theory we have

$$\frac{\frac{dF_1(r, T)}{dr}}{\frac{dF_3(r, T)}{dr}} = -3.$$

We have calculated the above ratio numerically from the lattice data and have found that for $T > 1.71T_c$ the deviation from the expected value (-3) are smaller than 10%.

IV. CONCLUSIONS

In this paper we have studied singlet and triplet static quark anti-quark correlators in finite temperature $SU(2)$

theory expressed in terms of Polyakov loop correlators and cyclic Wilson loops (cf. Eqs (3), (4)). The study of the latter is interesting as it has been used in resummed perturbative calculations of quarkonium spectral functions [30, 31]. In leading order and probably next-to-leading order of perturbation theory the static correlators defined by Eq. (3) and (4) give the energies of the singlet and triplet states respectively, however, this separation does not hold in general case. Due to interactions with ultrasoft fields there will be a mixing of singlet and triplet states which is proportional to $\alpha_s^3(1/r)$ and $(r\mu)^4$, with μ being the ultra-soft scale [27]. In our case the ultra-soft scale can be the binding energy, α_s/r , Λ_{QCD} or g^2T . Therefore it is expected that mixing is quite small at sufficiently small distances. We determined the mixing between singlet and triplet states in terms of the overlap factor $c_1(r)$. If the overlap factor is unity there is no mixing. Our lattice calculations show that $c_1(r)$ indeed approaches one at small distances. Using iterative APE smearing the deviation of $c_1(r)$ from unity can be largely reduced. Therefore the contribution of singlet state to $G_3(r, T)$ appears to be small at temperatures close to deconfinement temperature. This contribution is also controlled by the non-perturbative gap between the singlet and triplet states, i.e. the gap between the static potential and the first hybrid potential.

Our analysis shows that at short distances $rT < 1$ the singlet correlator is almost temperature independent, while the triplet correlator is largely affected by the deconfinement. The temperature dependence of the triplet correlators indicate the melting of the non-perturbative gap between the singlet and the triplet states above deconfinement, which turns out to be consistent with perturbative expectations. Because of the disappearance of the non-perturbative gap the small deviations of $c_1(r)$ from unity play no role in the deconfined phase. In particular, the difference between the singlet and triplet correlators defined through cyclic Wilson loops and using Coulomb gauge turns out to be quite small. This finding is important for application of thermal pNRQCD discussed in Ref. [28] to realistic quarkonia and temperatures not very far from the deconfinement temperature.

There are obvious extensions of the work carried out in this paper. One could do analogous calculations in $SU(3)$ gauge theory, however this hardly will give qualitatively different results. More interesting would be to extend the calculations to QCD with dynamical fermions. First steps in this direction are being made using improved staggered (p4) action [49]. It will be interesting to calculate the correlators $G_1(r, T)$ and $G_3(r, T)$ in perturbation theory beyond HTL approximation. One practical problem in doing these calculations is the fact that the scales T and m_D are not separated. This problem, however, could be possibly solved by using screened perturbation theory [50, 51, 52].

Acknowledgments

This work was supported by U.S. Department of Energy under Contract No. DE-AC02-98CH10886. The work of A.B. was supported by grants DOE DE-FC02-06ER-41439 and NSF 0555397. A.V. work was supported by the Joint Theory Institute funded together

by Argonne National Laboratory and the University of Chicago, and in part by the U.S. Department of Energy, Division of High Energy Physics and Office of Nuclear Physics, under Contract DE-AC02-06CH11357. We thank N. Brambilla, F. Karsch D. Teaney and A. Vairo for useful discussions.

-
- [1] T. Matsui and H. Satz, Phys. Lett. B **178**, 416 (1986)
- [2] T. Umeda, K. Nomura and H. Matsufuru, Eur. Phys. J. C **39S1**, 9 (2005) [arXiv:hep-lat/0211003].
- [3] M. Asakawa and T. Hatsuda, Phys. Rev. Lett. **92**, 012001 (2004) [arXiv:hep-lat/0308034].
- [4] S. Datta, F. Karsch, P. Petreczky and I. Wetzorke, Phys. Rev. D **69**, 094507 (2004) [arXiv:hep-lat/0312037].
- [5] P. de Forcrand *et al.* [QCD-TARO Collaboration], Phys. Rev. D **63**, 054501 (2001) [arXiv:hep-lat/0008005].
- [6] F. Karsch, E. Laermann, P. Petreczky, S. Stickan and I. Wetzorke, Phys. Lett. B **530**, 147 (2002) [arXiv:hep-lat/0110208].
- [7] M. Asakawa, T. Hatsuda and Y. Nakahara, Nucl. Phys. A **715**, 863 (2003) [Nucl. Phys. Proc. Suppl. **119**, 481 (2003)] [arXiv:hep-lat/0208059].
- [8] A. Jakovac, P. Petreczky, K. Petrov and A. Velytsky, Phys. Rev. D **75**, 014506 (2007) [arXiv:hep-lat/0611017].
- [9] L. D. McLerran and B. Svetitsky, Phys. Rev. D **24**, 450 (1981).
- [10] O. Kaczmarek, F. Karsch, E. Laermann and M. Lutgemeier, Phys. Rev. D **62**, 034021 (2000) [arXiv:hep-lat/9908010].
- [11] F. Karsch, E. Laermann and A. Peikert, Nucl. Phys. B **605**, 579 (2001) [arXiv:hep-lat/0012023].
- [12] P. Petreczky, O. Kaczmarek, F. Karsch, E. Laermann, S. Stickan, I. Wetzorke and F. Zantow, Nucl. Phys. A **698**, 400 (2002) [arXiv:hep-lat/0103034].
- [13] S. Nadkarni, Phys. Rev. D **34**, 3904 (1986).
- [14] O. Kaczmarek, F. Karsch, P. Petreczky and F. Zantow, Phys. Lett. B **543**, 41 (2002)
- [15] S. Digal, S. Fortunato and P. Petreczky, Phys. Rev. D **68**, 034008 (2003)
- [16] O. Kaczmarek, F. Karsch, F. Zantow and P. Petreczky, Phys. Rev. D **70**, 074505 (2004) [Erratum-ibid. D **72**, 059903 (2005)]
- [17] P. Petreczky and K. Petrov, Phys. Rev. D **70**, 054503 (2004)
- [18] O. Kaczmarek and F. Zantow, Phys. Rev. D **71**, 114510 (2005)
- [19] K. Petrov [RBC-Bielefeld Collaboration], hep-lat/0610041
- [20] S. Digal, P. Petreczky and H. Satz, Phys. Rev. D **64**, 094015 (2001) [arXiv:hep-ph/0106017].
- [21] C. Y. Wong, Phys. Rev. C **72**, 034906 (2005) [arXiv:hep-ph/0408020].
- [22] W. M. Alberico, A. Beraudo, A. De Pace and A. Molinari, Phys. Rev. D **72**, 114011 (2005) [arXiv:hep-ph/0507084].
- [23] A. Mocsy and P. Petreczky, Phys. Rev. D **73**, 074007 (2006) [arXiv:hep-ph/0512156].
- [24] D. Cabrera and R. Rapp, arXiv:hep-ph/0610254.
- [25] A. Mocsy and P. Petreczky, Phys. Rev. D **77**, 014501 (2008) [arXiv:0705.2559 [hep-ph]].
- [26] A. Mocsy and P. Petreczky, Phys. Rev. Lett. **99**, 211602 (2007) [arXiv:0706.2183 [hep-ph]].
- [27] N. Brambilla, A. Pineda, J. Soto and A. Vairo, Nucl. Phys. B **566**, 275 (2000) [arXiv:hep-ph/9907240].
- [28] N. Brambilla, J. Ghiglieri, A. Vairo and P. Petreczky, Phys. Rev. D **78**, 014017 (2008) [arXiv:0804.0993 [hep-ph]].
- [29] O. Jahn and O. Philipsen, Phys. Rev. D **70**, 074504 (2004) [arXiv:hep-lat/0407042].
- [30] M. Laine, O. Philipsen, P. Romatschke and M. Tassler, JHEP **0703**, 054 (2007) [arXiv:hep-ph/0611300].
- [31] M. Laine, O. Philipsen and M. Tassler, JHEP **0709**, 066 (2007) [arXiv:0707.2458 [hep-lat]].
- [32] Y. Burnier, M. Laine and M. Vepsalainen, JHEP **0801**, 043 (2008) [arXiv:0711.1743 [hep-ph]].
- [33] P. Petreczky, Eur. Phys. J. C **43**, 51 (2005) [arXiv:hep-lat/0502008].
- [34] S. Nadkarni, Phys. Rev. D **33**, 3738 (1986).
- [35] G. S. Bali, Phys. Rept. **343**, 1 (2001)
- [36] C. J. Morningstar, K. J. Juge, J. Kuti, Nucl. Phys. Proc. Suppl. **73**, 590 (1999)
- [37] K. J. Juge, J. Kuti, C. Morningstar, Phys. Rev. Lett. **90**, 161601 (2003)
- [38] C. Michael, S.J. Perantonis, J. Phys. G **18**, 1725 (1992)
- [39] M. Lüscher, P. Weisz, JHEP **09**, 010 (2001)
- [40] M. Albanese *et al.*, Phys. Lett. B **192**, 163 (1987)
- [41] J. Fingberg, U. M. Heller and F. Karsch, Nucl. Phys. B **392**, 493 (1993) [arXiv:hep-lat/9208012].
- [42] S.P. Booth *et al.* [UKQCD Coll.], Phys. Lett. B **275**, 424 (1992)
- [43] O. Philipsen, Phys. Lett. B **535**, 138 (2002) [arXiv:hep-lat/0203018].
- [44] O. Kaczmarek, F. Karsch, P. Petreczky and F. Zantow, Nucl. Phys. Proc. Suppl. **129**, 560 (2004) [arXiv:hep-lat/0309121].
- [45] G. P. Lepage, P. B. Mackenzie, Phys. Rev. D **48**, 2250 (1992)
- [46] A. K. Rebhan, Phys. Rev. D **48**, 3967 (1993); Nucl. Phys. B **430**, 319 (1994)
- [47] U. M. Heller, F. Karsch and J. Rank, Phys. Rev. D **57**, 1438 (1998) [arXiv:hep-lat/9710033].
- [48] This follows from the multipole expansion of singlet and triplet interpolating fields performed in Ref. [27], cf. Eq. (6) of Ref. [27]. We thank A. Vairo for clarifying this point.
- [49] RBC-Bielefeld Collaboration, work in progress
- [50] F. Karsch, A. Patkós and P. Petreczky, Phys. Lett. B **401**, 69 (1997)
- [51] J. O. Andersen, E. Braaten and M. Strickland, Phys. Rev. Lett. **83**, 2139 (1999)

r	$N_s = 24$			$N_s = 32$		
	c_1^a	E_1	$\frac{\chi^2}{\text{dof}}$	c_1^a	E_1	$\frac{\chi^2}{\text{dof}}$
1	1.00077(28)	0.33524(2)	0.50	1.00046(28)	0.33522(1)	1.48
2	1.0049(13)	0.48423(8)	0.49	1.0039(12)	0.48415(6)	0.96
3	1.0134(45)	0.56568(24)	0.64	1.0115(32)	0.56550(16)	0.93
4	1.027(10)	0.62400(61)	0.73	1.0237(67)	0.62365(35)	0.75
5	1.049(22)	0.6732(14)	1.23	1.038(14)	0.67232(78)	0.66
6	1.067(43)	0.7171(27)	1.43	1.051(29)	0.7161(17)	1.10
7	1.087(91)	0.7582(59)	1.80	1.023(60)	0.7542(40)	1.53
8	1.05(16)	0.793(11)	2.06	0.93(11)	0.7861(83)	1.69

TABLE II: Single exponential fit of $G(r, T)$ at $\beta = 2.5$ using $N_\tau = 12 - 24$ for two spatial sizes $N_s = 24$ and $N_s = 32$.

r	c_1^a	E_1	$\frac{\chi^2}{\text{dof}}$
1	1.00065(44)	0.28580(2)	0.64
2	1.0084(28)	0.39584(12)	1.21
3	1.0325(90)	0.44727(36)	0.90
4	1.078(21)	0.47939(80)	0.54
5	1.143(39)	0.5038(14)	0.41

TABLE III: Single exponential fit of $G(r, T)$ at $\beta = 2.7$ using $N_t = 20 - 28$.

[52] J. P. Blaizot, E. Iancu and A. Rebhan, Phys. Rev. Lett. **83**, 2906 (1999)

Appendix

In this appendix we give some details of the fits of the overlap factors and energy levels for different lattice volumes.

Let us first discuss the fits of the color averaged correlator $G(r, T)$. We have fitted our lattice data at low temperatures with one exponential form $G(r, T) = c_1^a(r) \exp(-E_1(r)/T)$. For $\beta = 2.5$ we used lattices with temporal extent $N_\tau = 12, 14, 16, 18, 20, 22$ and 24 . For $\beta = 2.7$ we used $N_\tau = 20, 22, 24$ and 28 . The values of fit parameters $c_1^a(r)$ and $E_1(r)$ are shown in Table II for $\beta = 2.5$ and Table III for $\beta = 2.7$. As one can see from the Tables at $\beta = 2.5$ the single exponential fit works reasonably well up to distance $r = 7$ for $N_s = 32$ and distance $r = 6$ for $N_s = 24$. At $\beta = 2.7$ the fits work up to distance $r = 5$ only. We also performed double exponential fits $G(r, T) = \exp(-E_1(r)/T) + \exp(-E_2(r)/T)$ to check the reliability of the extraction of E_1 . The results are shown in Tables IV and V for $\beta = 2.5$ and $\beta = 2.7$ respectively. Overall the values of E_1 extracted from 2-exponential fits are in reasonably good agreement with the corresponding values extracted from singlet exponential fit.

We fitted the singlet correlators calculated for different number of APE smearing steps with single exponential Ansatz $G_1(r, T) = c_1(r) \exp(-E_1(r)/T)$. The results for

r	$N_s = 24$			$N_s = 32$		
	E_1	E_2	$\frac{\chi^2}{\text{dof}}$	E_1	E_2	$\frac{\chi^2}{\text{dof}}$
1	0.335204(5)	1.011(41)	0.89	0.335199(3)	1.048(50)	0.84
2	0.483974(18)	0.989(20)	0.56	0.483948(9)	0.998(15)	0.47
3	0.565022(42)	0.983(17)	0.44	0.564946(29)	0.982(14)	0.60
4	0.62269(12)	0.984(21)	0.55	0.622522(88)	0.986(19)	0.80
5	0.67088(42)	0.987(36)	1.08	0.67046(19)	1.003(24)	0.65
6	0.7140(10)	1.004(57)	1.35	0.71357(48)	1.023(40)	0.86
7	0.7545(24)	1.016(86)	1.69	0.7533(12)	1.07(10)	1.43

TABLE IV: Double exponential fit of $G(r, T)$ at $\beta = 2.5$ using $N_\tau = 12 - 24$ for two spatial sizes $N_s = 24$ and $N_s = 32$.

r	E_1	E_2	$\frac{\chi^2}{\text{dof}}$
1	0.285780(1)	0.700(11)	0.14
2	0.395551(9)	0.6819(60)	0.15
3	0.446179(27)	0.6657(45)	0.11
4	0.476943(53)	0.6532(33)	0.07
5	0.49965(12)	0.6445(37)	0.07
6	0.51857(29)	0.6362(48)	0.11
7	0.53545(67)	0.6297(63)	0.16
8	0.5514(14)	0.6240(79)	0.18

TABLE V: Double exponential fit of $G(r, T)$ at $\beta = 2.7$ using $N_\tau = 20 - 28$.

the fit parameters $c_1(r)$ and $E_1(r)$ at $\beta = 2.5$ are shown in Tables VI and VII for zero and 10 APE smearing steps respectively. In Tables VIII, IX and X we show the fit parameters for $\beta = 2.7$ and zero, 10 and 20 APE smearing steps.

r	$N_s = 24$			$N_s = 32$		
	c_1	E_1	$\frac{\chi^2}{\text{dof}}$	c_1	E_1	$\frac{\chi^2}{\text{dof}}$
1	0.89076(34)	0.33523(2)	0.36	0.89043(28)	0.33521(2)	1.31
2	0.68239(89)	0.48406(8)	0.77	0.68191(79)	0.48401(6)	0.70
3	0.5113(16)	0.56549(20)	0.20	0.5095(14)	0.56519(14)	1.11
4	0.4020(33)	0.62353(53)	0.19	0.4035(24)	0.62360(33)	0.58
5	0.3439(63)	0.6731(12)	0.82	0.3367(46)	0.67123(86)	0.34
6	0.313(14)	0.7174(32)	2.24	0.312(10)	0.7173(21)	1.32
7	0.321(32)	0.7642(74)	1.93	0.261(20)	0.7496(54)	1.10
8	0.311(46)	0.803(11)	0.70	0.240(38)	0.786(11)	3.19
9	0.35(13)	0.845(29)	1.43	0.228(79)	0.822(24)	1.69

TABLE VI: Single exponential fit of $G_1(r, T)$ at different lattice separations r at $\beta = 2.5$ with no APE smearing using $N_\tau = 12 - 24$.

r	$N_s = 24$			$N_s = 32$		
	c_1	E_1	$\frac{\chi^2}{\text{dof}}$	c_1	E_1	$\frac{\chi^2}{\text{dof}}$
1.0000	0.99457(96)	0.33528(6)	0.71	0.99260(50)	0.33516(3)	0.53
1.4142	0.9926(19)	0.42930(11)	0.81	0.9904(11)	0.42916(6)	0.32
1.7320	0.9886(26)	0.47322(16)	0.38	0.9864(16)	0.47310(9)	0.33
2.0000	0.9919(30)	0.48414(17)	0.70	0.9882(18)	0.48389(10)	0.19
2.8284	0.9810(69)	0.55824(42)	0.53	0.9721(40)	0.55758(24)	0.32
3.0000	0.9835(63)	0.56554(36)	0.50	0.9751(46)	0.56494(27)	0.28
3.4641	0.954(10)	0.59681(68)	0.72	0.9487(60)	0.59643(37)	0.47
4.0000	0.972(13)	0.62406(82)	0.33	0.9503(98)	0.62243(60)	0.19
4.2426	0.950(16)	0.6376(11)	0.33	0.938(11)	0.63656(70)	0.32
5.0000	0.953(26)	0.6732(17)	0.83	0.923(18)	0.6706(12)	0.40
5.1961	0.891(28)	0.6803(21)	1.47	0.870(16)	0.6787(11)	0.72
5.6568	0.897(40)	0.7015(32)	0.94	0.880(25)	0.7000(18)	0.12
6.0000	0.933(44)	0.7185(31)	0.48	0.877(35)	0.7129(26)	0.54
6.9282	0.765(66)	0.7473(61)	1.34	0.807(41)	0.7508(33)	0.88
7.0000	0.837(68)	0.7550(61)	0.62	0.874(64)	0.7563(49)	0.38
7.0711	0.902(87)	0.7643(71)	0.99	0.808(52)	0.7568(44)	0.29
8.0000	0.71(11)	0.786(11)	1.28	0.86(10)	0.7963(80)	1.78

TABLE VII: Single exponential fit of $G_1(r, T)$ at $\beta = 2.5$ calculated with 10 steps of APE smearing using $N_\tau = 12 - 24$.

r	c_1	E_1	$\frac{\chi^2}{\text{dof}}$
1	0.89048(47)	0.28578(2)	2.72
2	0.6898(18)	0.39557(11)	2.30
3	0.5241(39)	0.44628(31)	2.29
4	0.4243(73)	0.47792(72)	1.66
5	0.371(12)	0.5019(14)	1.44
6	0.362(21)	0.5238(25)	0.83
7	0.385(33)	0.5449(36)	0.36
8	0.396(46)	0.5612(48)	1.04
9	0.497(76)	0.5838(64)	0.74
10	0.55(11)	0.5991(89)	0.59

TABLE VIII: Single exponential fit of $G_1(r, T)$ at $\beta = 2.7$ with no APE smearing using $N_\tau = 20 - 28$.

r	c_1	E_1	$\frac{\chi^2}{\text{dof}}$
1.0000	0.9962(12)	0.28582(5)	0.02
1.4142	0.9952(25)	0.35819(10)	1.00
1.7320	0.9927(33)	0.38969(14)	0.59
2.0000	0.9923(42)	0.39585(18)	0.18
2.8284	0.9798(97)	0.44311(42)	1.74
3.0000	0.978(11)	0.44681(45)	0.59
3.4641	0.971(14)	0.46541(62)	1.19
4.0000	0.968(20)	0.47854(88)	0.41
4.2426	0.949(24)	0.4852(11)	1.08
5.0000	0.944(34)	0.5018(15)	0.22
5.1961	0.949(37)	0.5073(17)	0.89
5.6568	0.921(48)	0.5151(22)	1.02
6.0000	0.920(52)	0.5211(24)	0.04
6.9282	0.939(76)	0.5398(34)	0.78
7.0000	0.894(78)	0.5381(37)	0.20
7.0711	0.894(72)	0.5399(34)	0.60
8.0000	0.849(99)	0.5522(50)	0.02
8.4853	0.86(11)	0.5614(57)	0.30
8.6603	0.89(14)	0.5661(64)	0.37
9.0000	0.78(13)	0.5640(73)	0.24
9.8995	0.80(18)	0.5793(94)	0.07
10.0000	0.75(17)	0.5767(98)	0.19
10.3923	0.74(19)	0.584(11)	0.25

TABLE IX: Single exponential fit of $G_1(r, T)$ at $\beta = 2.7$ calculated with 10 steps of APE smearing using $N_\tau = 20 - 28$.

r	c_1	E_1	χ^2/dof
1.0000	0.9965(15)	0.28582(6)	1.21
1.4142	0.9965(26)	0.35809(11)	1.10
1.7320	0.9957(45)	0.38949(19)	2.02
2.0000	0.9982(53)	0.39573(22)	1.29
2.8284	0.993(12)	0.44262(51)	1.05
3.0000	0.993(13)	0.44639(55)	1.38
3.4641	0.985(21)	0.46418(88)	3.86
4.0000	0.985(24)	0.4771(10)	2.50
4.2426	0.979(31)	0.4839(13)	0.65
5.0000	0.979(38)	0.4999(16)	2.64
5.1962	0.984(48)	0.5049(20)	3.10
5.6569	0.992(58)	0.5139(25)	0.86
6.0000	0.982(63)	0.5193(27)	2.34
6.9282	1.04(10)	0.5378(40)	2.29
7.0000	0.983(86)	0.5360(37)	2.10
7.0711	1.03(11)	0.5395(44)	0.86
8.0000	1.00(12)	0.5525(52)	2.15
8.4853	1.11(18)	0.5640(70)	1.08
9.0000	0.94(15)	0.5642(69)	1.67
10.0000	0.92(22)	0.577(10)	1.82

TABLE X: Single exponential fit of $G_1(r, T)$ at $\beta = 2.7$ calculated for 20 APE smearing using $N_\tau = 20 - 28$.